Atom counting in ultracold gases using photoionization and ion detection

T. Campey,* C. J. Vale, M. J. Davis, N. R. Heckenberg, and H. Rubinsztein-Dunlop
School of Physical Sciences, The University of Queensland, Brisbane, Queensland 4072, Australia

S. Kraft, C. Zimmermann, and J. Fortágh
Physikalisches Institut der Universität Tübingen, 72076 Tübingen, Germany
(Received 6 July 2006; published 18 October 2006)

We analyze photoionization and ion detection as a means of accurately counting ultracold atoms. We show that it is possible to count clouds containing many thousands of atoms with accuracies better than $N^{-1/2}$ with current technology. This allows the direct probing of sub-Poissonian number statistics of atomic samples. The scheme can also be used for efficient single-atom detection with high spatiotemporal resolution. All aspects of a realistic detection scheme are considered, and we discuss experimental situations in which such a scheme could be implemented.

DOI: 10.1103/PhysRevA.74.043612 PACS number(s): 03.75.Be, 32.80.Fb, 39.90.+d

I. INTRODUCTION

The term "atom optics" arises from the analogy between experiments exhibiting the wavelike properties of light with those demonstrating the wavelike properties of matter [1]. Due to the vanishingly small de Broglie wavelength of room-temperature atoms it is necessary to cool gases to microkelvin temperatures before these properties are observable. Before 1995, experiments in atom optics used clouds of laser-cooled thermal atoms that can be considered similar to thermal light sources in optics, with coherence lengths of less than 1 μm.

The realization of Bose-Einstein condensation (BEC) in 1995 [2–4] provided the first intense sources of coherent matter waves, analogous to the invention of the optical laser. Many of the early experiments with BECs concentrated on their wavelike properties, which in general can be well described by the Gross-Pitaevskii equation for the classical field $\psi(x) \approx \langle \hat{\Psi}(x) \rangle$. Some notable experiments include the interference of independently prepared condensates [5] and the demonstration of atom lasers [6–9]. These experiments rely on the first-order coherence of the condensate, and in some sense can be considered to be coherent "classical atom optics."

Recently there have been an increasing number of experiments focusing on the generation and measurement of nontrivial higher-order coherences in matter waves that are beyond the scope of Gross-Pitaevskii mean-field theory. These experiments could be said to be in the area of "quantum atom optics" [10]. The development of this new area bears a close resemblance to the development of quantum optics following the invention of the optical laser. Just as quantum optics relies on single-photon detectors, quantum atom optics will utilize detectors with single-atom resolution, such as the technique we describe in this paper.

One of the earliest experiments probing higher-order coherence in BECs was in the measurement of three-body loss from a BEC, from which the correlation function $g^{(3)}(\mathbf{x})$ could be inferred [11]. There have been several measurements made of the local second-order correlation function $g^{(2)}(\mathbf{x})$ for a number of systems, including a one-dimensional (1D) strongly interacting Bose gas [12,13], a quasicondensate [14], and a thermal Bose gas [15]. The value of $g^{(2)}(\mathbf{x})$ for an atom laser has been measured in Ref. [16].

There has also been strong interest in relative number squeezing. This is where a state is generated in which the number difference between two or more atomic samples is sub-Poissonian. Javanainen and Ivanov [17] showed that splitting condensates by adiabatically turning up a tunnel barrier can produce number-squeezed atomic states. Experimentally, Orzel *et al.* [18] loaded a BEC into a one-dimensional optical lattice and observed the degradation of interference fringes. This was interpreted to be caused by increased phase fluctuations due to reduced number fluctuations at the lattice sites. A similar observation was made in the first demonstration of a 3D Mott insulator state [19] and further elucidated by other related experiments [20].

Correlations and relative number squeezing have been predicted in collisions and four-wave mixing in condensates [21–24], as well as in down-conversion of a molecular BEC in both the spontaneous [25] and stimulated [26] regimes. While experiments have observed four-wave mixing processes [27,28] and matter-wave amplification [29], there has been no direct measurement of these correlations.

Experimentally, other high-order correlations have been directly detected by suitable analysis of absorption images from an ensemble of experiments [30,31]. Other schemes such as the "quantum tweezer" [32] can deterministically extract sub-Poissonian atomic samples from a BEC. Optical dipole traps along with fluorescence imaging have been used to demonstrate sub-Poissonian statistics in small samples of atoms [33].

In order to directly probe atom number statistics of cold quantum gases, one would ideally like an atom counter with accuracy at the single-atom level. Existing single-atom detection schemes can be divided into two categories: optical and contact. One of the simplest optical schemes is based on resonance fluorescence detection [33–35]. Assuming negligible background, the shot-noise-limited atom number uncer-

*Electronic address: t.campey@uq.edu.au

tainty in a fluorescence measurement scales as $\sqrt{N/\alpha\gamma\tau}$, where N is the number of atoms, α is the collection efficiency of the detector, γ is the mean scattering rate, and τ is the integration time [36]. With a long enough integration time it is possible to measure atom numbers with sub-Poissonian precision. However, limitations such as atom heating restrict the capability of sub-Poissonian fluorescence detection to atom numbers of order <100 [33]. Absorption measurements offers more favorable scaling to higher atom numbers [36] but achieving good absolute accuracy remains technically difficult. High-finesse optical cavities offer excellent sensitivity for single-atom detection [37–39] and can be used for slow counting of a large number of atoms. Cavities offer an improvement in signal to noise of $\sqrt{\mathcal{F}}$, where $\mathcal{F}$ is the cavity finesse, compared to single-pass measurements for a fixed amount of heating [40,41]. Moderate cavities have also been shown to aid fluorescence and absorption measurements [36]. It is difficult, however, to apply cavity techniques to counting large atom numbers and long integration times are required.

The second category of single-atom detectors is based on contact methods. These generally involve a charged-particle or metastable atom with high internal energy impacting on a charged-particle detector. This initiates a cascade of electron emissions, which are amplified to produce a macroscopic current pulse. This method is particularly useful for detecting metastable He atoms [42] where the arrival statistics of atoms released from a BEC allowed for matter-wave Hanbury-Brown Twiss correlations to be observed [15]. While this detection method is simple, metastable atoms remain difficult to condense and most cold atom experiments use alkali-metal atoms.

In this paper we describe an atom detection scheme based on photoionization and ion detection. This scheme overcomes some of the difficulties associated with optical detection, can be applied to ground-state alkali-metal atoms, and is capable of extending sub-Poissonian counting to much larger numbers of atoms. Photoionization [43] and ionization [44] have previously been considered as a means of efficient atom detection. However, these proposals have not included many factors present in realistic detectors. First we note that the best absolute detection efficiencies of room-temperature charged-particle detectors are of order 0.8–0.9 [45,46]. (Superconducting tunnel junctions can in principle provide unity detection efficiency [47] but are impractical for many experimental setups.) This has serious consequences for any experiment that endeavors to count a large number of atoms, but as we show in this paper, provided the detection efficiency is greater than 0.5, it is still possible to count atoms with accuracies better than $1/\sqrt{N}$. The achievable accuracy depends on several factors including the detector calibration, background count rates, detector pulse resolution times, ionization rates, and the uncertainties in these parameters, all of which are included in our analysis.

This paper is organized as follows. In Sec. II we describe the experimental arrangement necessary for atom counting and how it can be applied to a cloud of trapped ^{87}Rb atoms. Section III addresses the statistics associated with the detection scheme along with the requirements on the detector efficiency. In Sec. IV we discuss detector calibration and describe numerical simulations of the calibration including the effects mentioned above. Section V looks at the application of the scheme in the presence of losses and we follow with a discussion of potential applications. Appendixes A and B contain derivations of certain expressions used in the paper.

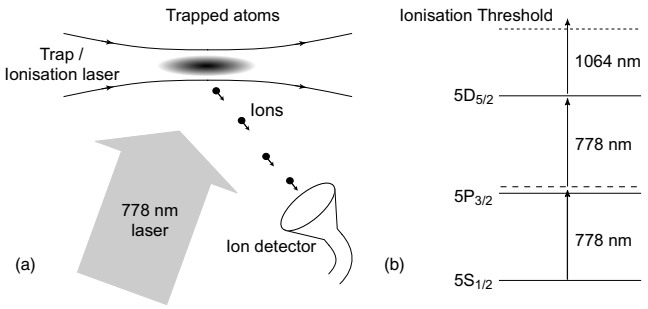

FIG. 1. (a) In the proposed atom-counting scheme atoms are ionized from an optical dipole trap via a three-photon process. The resulting ions are accelerated into an ion detector. (b) The ionization scheme showing the relevant energy levels of ^{87}Rb (not to scale). The scheme consists of 2×778 nm photon excitation to the $5D_{5/2}$ state, followed by ionization with a Nd:YAG laser, which also forms the dipole trap.

II. SCHEME

The method we propose consists of slowly photoionizing a sample of atoms and accelerating the ions to a charged-particle detector. Figure 1(a) shows the elements of the scheme. A cloud of cold atoms is held in an optical dipole trap where it is illuminated by the ionization lasers. Our discussion focusses specifically on the case of ^{87}Rb atoms but the scheme could be modified to detect other alkali-metal atoms by the correct choice of lasers. Figure 1(b) shows the relevant energy levels and transitions for ^{87}Rb.

The ionization scheme consists of two stages. The first is two-photon excitation with a low-intensity 778 nm laser from the $5S_{1/2}$ state to the $5D_{5/2}$ state. The second is ionization from this state with a high-intensity infrared laser such as a neodymium-doped yttrium aluminum garnet (Nd:YAG) laser. The $5D_{5/2}$ state has a photoionization cross section approximately three orders of magnitude higher than the ground state [48] so ionization can readily be achieved with a cw laser of wavelength shorter than $\sim$1200 nm rather than with pulsed lasers [49]. Ion detection is achieved after appropriate ion collection optics using a standard ion detector such as a channel electron multiplier (CEM) or discrete dynode detector.

The atom-counting scheme works best if the pulses produced by ions striking the ion detector are well resolved in time. This means the ionization rate $\dot{N}_I$ should be much lower than the inverse of the pulse resolution time of the detection system $1/\tau_r$. In Sec. V we will see that this means that for typical detector efficiencies and trap lifetimes, and atom numbers of the order of 10^3 or 10^4, the ionization should take place on a time scale of order several milliseconds. In order to confine the atoms during this time, the Nd:YAG laser is focused to create a dipole trap. This local-

izes the atoms in the highest-intensity region of the beam. The intensity must be high enough to produce a trap sufficiently deep that no atoms are lost due to heating as the ionization takes place. The major source of heating is the spontaneous decay of atoms excited to the $5D_{5/2}$ state. A high Nd:YAG laser intensity thus helps eliminate trap loss not only by creating a deep trap, but also by ensuring that an atom excited to the $5D_{5/2}$ state has a substantially higher probability of being ionized than of decaying back to the ground state. Atoms that decay from the $5D_{5/2}$ state can end up in several ground-state sublevels. A benefit of the dipole trap is that it traps all of these sublevels, in contrast to magnetic fields, which can only trap a restricted class of sublevels.

The rate of ionization can be controlled with the 778 nm laser intensity. In Sec. V we show that for a given atom number and trap loss rate there is an optimal ionization rate that minimizes the uncertainty in the inferred atom number. In order to hold the ionization rate approximately constant at the ideal value, the 778 nm laser intensity can be exponentially ramped to compensate for the reduction in trapped atom number as ions are produced. However, we also show that the scheme works well with constant laser intensities.

This state-selective scheme also represents an efficient single-atom detector [53]. The ionization lasers can be tightly focussed to detect atoms at a well-defined spatial location. The two-photon excitation rate is proportional to the squared intensity of the 778 nm laser so that scattered light is less likely to heat atoms not in the detection region. Additionally, for single-atom detection the spatial intensity profiles of the two lasers can be chosen so that the repulsive optical dipole potential of the blue-detuned 778 nm laser can be compensated for by the attractive potential of the high-power red-detuned ionizing laser. This leads to minimal perturbation of undetected atoms, which may for instance be magnetically detuned or trapped in a different internal state. These factors, and the relatively quick ionization times, make this a flexible scheme well suited to single-atom detection with excellent spatiotemporal resolution.

III. COUNTING WITH IMPERFECT DETECTORS

We now consider how accurately an atom number can be determined using a scheme in which ions are counted with a nonunity-efficiency detector. The overall ion detection efficiency is

$$\eta_i = \eta_{det} p_r, \tag{1}$$

where η_{det} is the efficiency of the ion detection system and is the product of the ion detector efficiency η'_{det} and the collection efficiency η_{coll}. The quantity p_r is the probability that an ion is temporally resolvable from the other ions detected, and is ionization rate dependent.

If N_I ions are produced, the number of ions counted, N_i, is described by a binomial distribution. Provided $\eta_i(1-\eta_i)N_I$ is greater than ~ 5, this is well approximated by a normal distribution with mean $\eta_i N_I$ and standard deviation $\sqrt{\eta_i(1-\eta_i)N_I}$ [50]. In a given experiment, the number of atoms ionized can be inferred to be

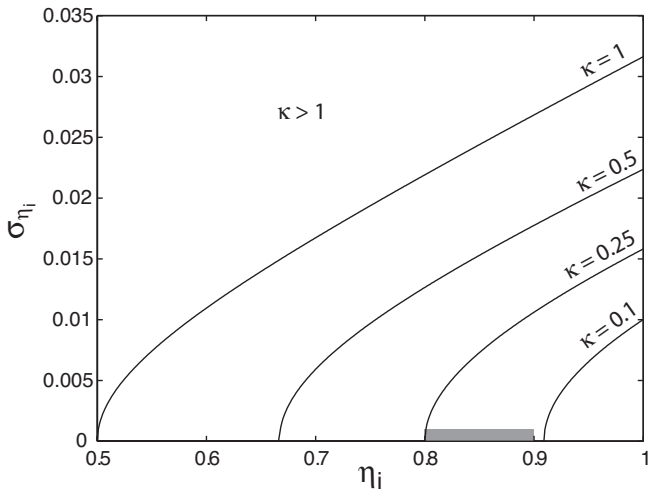

FIG. 2. Contours of the normalized count uncertainty κ for an atom-counting system with ion detection efficiency $\eta_i \pm \sigma_{\eta_i}$, for ion number $N_I = 10^3$. The shaded area shows the region of parameter space expected for common commercial ion detectors calibrated as detailed in Sec. IV.

$$N_{I,inf} = \frac{N_i}{\eta_i}, \tag{2}$$

with an uncertainty

$$\sigma_{N_{I,inf}} = \sqrt{\frac{N_i(1-\eta_i)}{\eta_i^2} + \frac{N_i^2 \sigma_{\eta_i}^2}{\eta_i^4}}, \tag{3}$$

where σ_{η_i} is the uncertainty in η_i.

In order to compare this uncertainty to Poissonian fluctuations, we define the normalized count uncertainty:

$$\kappa \equiv \frac{\sigma_{N_{I,inf}}^2}{N_{I,inf}}. \tag{4}$$

The quantity κ is related to the measurement Fano factor discussed in Sec. VI but includes an additional systematic contribution due to the uncertainty in the detection efficiency [the second term under the square root in Eq. (3)]. $\kappa = 1$ implies the count uncertainty is equal to the uncertainty inherent in Poissonian statistics. In order to count ions with error less than $\sqrt{N_I}$, κ must be less than 1.

In Fig. 2, contours of the normalized count uncertainty κ are plotted as a function of η_i and σ_{η_i} for $N_I = 10^3$. From this figure it can be seen that for a detection system in which the detection efficiency is known exactly, i.e., $\sigma_{\eta_i} = 0$, the overall ion detection efficiency η_i need only be greater that 50% to achieve κ less than 1. As the uncertainty in the detection efficiency increases, the required detection efficiency to achieve $\kappa \leqslant 1$ also increases. Thus, to achieve a low value of κ, we require a high-efficiency detector that is well calibrated. In the next section we examine how this can be done.

IV. DETECTOR CALIBRATION

To infer the number of atoms ionized and its uncertainty from an ion count, we need to know the overall ion detection

efficiency η_i and its uncertainty σ_{η_i}. From Eq. (1) this means we need to know the ion detection system efficiency η_{det} and the ion temporal resolution probability p_r, each with their respective uncertainties. We first consider how to measure η_{det} to high accuracy, or in other words, how to calibrate the ion detection system.

Accurate calibration can be achieved by means of a scheme in which an additional detector is used to count the electrons produced by ionization [51]. If N_I atoms are ionized in a calibration, and the overall ion and electron detection efficiencies are η_i and η_e, respectively [where, analogously to Eq. (1), $\eta_e = \eta_{det,e} p_{r,e}$], then

$$N_i = \eta_i N_I, \tag{5}$$

$$N_e = \eta_e N_I, \tag{6}$$

$$N_c = \eta_i \eta_e N_I, \tag{7}$$

where N_i is the number of ions counted, N_e is the number of electrons counted, and N_c is the number of ion-electron coincidences counted. Therefore

$$\eta_i = \frac{N_c}{N_e}, \tag{8}$$

which shows that only the coincidence and electron counts are required to find the ion detection efficiency; we do not need to know the efficiency of the electron detector.

In order to count the number of coincidences, it is first necessary to specify how coincidences are identified. In general there will be a distribution of times taken for ions to move from the region of ionization to striking the detector and producing a pulse. The width of this distribution will depend on the range of initial velocities of the ions and the variation in electric field at different locations within the atom cloud. The same is true for the electrons. There will therefore be a distribution of intervals between ions and their corresponding electrons. With modern pulse counting electronics it is straightforward to produce lists of the arrival times of electrons and ions with precisions on the order of 100 ps [52] and these can be used to generate a list of intervals between electrons and the following ions. If a histogram of these intervals is plotted, true coincidences will appear as a peak against a small background of false coincidences. This peak can then be used to define a window for true coincidences.

The coincidence window may also contain false coincidences, which occur when an unpartnered ion (i.e., one for which the corresponding electron was not detected) arrives within the window of an unpartnered electron. Also, due to the finite size of the window, some true coincidences may not be counted. The mean net number of false coincidences $\bar{N}_f$ and its uncertainty σ_f are derived in Appendix A.

In order to take false coincidences and background ions and electrons into account in the ion detection efficiency, we define corrected ion, electron and coincidence counts as $N_i' \equiv N_i - \bar{N}_{ib}$, $N_e' \equiv N_e - \bar{N}_{eb}$, and $N_c' \equiv N_c - \bar{N}_f$, respectively. $\bar{N}_{ib}$ and $\bar{N}_{eb}$ are respectively the mean numbers of background ions and electrons counted in the calibration period and can be measured by counting ions and electrons in the absence of the calibration atoms. The overall ion detection efficiency is then

$$\eta_i = \frac{N_c'}{N_e'}. \tag{9}$$

The ion detection efficiency given by Eq. (9) is the value that applies in a calibration and is valid for the ionization rate used in the calibration. To find the system ion detection efficiency (which is ionization rate independent) we need to correct η_i for the value of the ion temporal resolution probability p_r that applies in the calibration. From Eqs. (1) and (9), the system ion detection efficiency is

$$\eta_{det} = \frac{N_c'}{N_e' p_r}, \tag{10}$$

and from Appendix B

$$p_r = 1 - \tau_r \dot{N}_i - \frac{1}{2}(\tau_r \dot{N}_i)^2, \tag{11}$$

where τ_r is the minimum time interval for which two ions can be resolved from each other, and $\dot{N}_i$ is the average rate of ion detection in the calibration.

We also need to determine the uncertainty in η_{det}. This uncertainty arises mainly from the fact that for a given number of atoms ionized, the number of ion, electron and coincidence counts are described by binomial distributions. An additional contribution comes from the uncertainties in the number of background electrons and false coincidences counted during the calibration. Taking all of these effects into account, and for values of p_r close to unity, the uncertainty in the ion detection system efficiency is

$$\sigma_{\eta_{det}} = \frac{N_c'}{N_e'} \sqrt{\left(\frac{1}{N_c'} - \frac{1}{N_e'}\right) + \frac{\sigma_{eb}^2}{N_e'^2} + \frac{\sigma_f^2}{N_c'^2}}, \tag{12}$$

where σ_{eb} is the uncertainty in the number of background electrons counted and is equal to $\sqrt{\bar{N}_{eb}}$, assuming the detection of background electrons is a Poisson process.

To minimize the uncertainty in the ion detection efficiency, it is desirable to minimize background counts. Background electrons and ions arise from three main potential sources. The vacuum gauges and ion getter pumps commonly used in ultracold-atom experiments work by ionizing atoms and hence some of the ionization products may find their way to the detector. While the vacuum gauge can simply be turned off during the experiment, ion counts from the pump can be reduced by adding appropriate shielding. The third potential source of background ions and electrons is the ionization by stray laser light of the Rb atoms covering the interior of the vacuum chamber.

Background ions and electrons can be prevented from reaching the detectors by using suitable ion optics, such as the apparatus presented in [53]. In this apparatus four electrodes are used to accelerate and focus ions and guide them to the detector. The ion trajectories were calculated using standard software and it was found that only a volume of ~ 1 cm^3 is imaged onto the detector. Ions produced outside

of this volume are not detected and it is estimated that background counts can be almost entirely suppressed.

From Appendix A, the uncertainty in the number of false coincidences can also be made very small. From Eqs. (10) and (12), neglecting background counts and false coincidences, and for $p_r \approx 1$, the average relative uncertainty in the ion detection efficiency is

$$\frac{\sigma_{\eta_{det}}}{\eta_{det}} = \sqrt{\frac{1-\eta_{det}}{\eta_{det}\eta_{det,e}N_I}}. \tag{13}$$

For calibration parameters $\dot{N}_I = 10^5\ \mathrm{s}^{-1}$, $\eta_{det} = \eta_{det,e} = 0.8$, and a calibration time of $\tau_{cal} = 10$ s, this expression is accurate to within 1% for background electron and ion rates of up to $10^3\ \mathrm{s}^{-1}$. Equation (13) shows that this calibration method works best for large atom numbers and high overall ion and electron detection efficiencies.

In order to test the values for η_{det} and $\sigma_{\eta_{det}}$ predicted by the calibration equations, numerical simulations of calibration experiments were carried out. These simulations included all the relevant features of a real calibration, such as ionization following Poissionian statistics, detection of ions and electrons subject to their respective detection efficiencies, background electrons and ions, resolution times of the detectors, generation of a coincidence window from the lists of electron and ion arrival times, and use of the coincidence window to determine the number of coincidences.

Each simulation generated electron, ion, and coincidence counts for both "real" and background electrons and ions. Then, as would be done in a real calibration experiment, the corrected counts were calculated using the estimated numbers of background electrons, background ions, and false coincidences. An inferred value and an inferred uncertainty of the ion detection system efficiency η_{det} were then found using Eqs. (10) and (12).

Excellent agreement was found between the theory and simulation for a wide range of values. Figure 3 shows a histogram of the inferred ion detection efficiency for 1000 runs of the simulation with $\eta_{det} = \eta_{det,e} = 0.9$, $\dot{N}_I = 10^4\ \mathrm{s}^{-1}$, $\tau_{cal} = 10$ s, $\tau_r = 10$ ns, and $\dot{N}_{ib} = \dot{N}_{eb} = 10^2\ \mathrm{s}^{-1}$. The inferred values of η_{det} have a mean of 0.899 993 in excellent agreement with the actual value of 0.9. The standard deviation of the inferred values was 1.047×10^{-3}, also in excellent agreement with the average theoretical value of $\sigma_{\eta_{det}}$, which for these parameters is 1.049×10^{-3}.

To determine the values of η_i and σ_{η_i} that apply in a counting experiment, the calibrated values of η_{det} and $\sigma_{\eta_{det}}$ must be corrected for the value of the ion temporal resolution probability p_r that applies for the ion detection rate used in the experiment. η_i is found from Eq. (1) and $\sigma_{\eta_i} = \sigma_{\eta_{det}}$ for $p_r \approx 1$. For the case of ionization at a constant rate in atoms per second, p_r is given by Eq. (B7) in Appendix B. If ionization occurs at a constant per atom rate (i.e., ionizing laser powers are held constant), we use the effective ion resolution probability p_r', given by Eq. (B11). It should be noted that for the calibration to be valid, the ion collection efficiency η_{coll} must remain constant between calibration and experiment. This could be achieved by calibrating using cold atoms in the same trap as used in the experiment. To achieve the lowest possible uncertainty in the atom count, η_{coll} should be unity, which can in principle be achieved with well-designed ion optics.

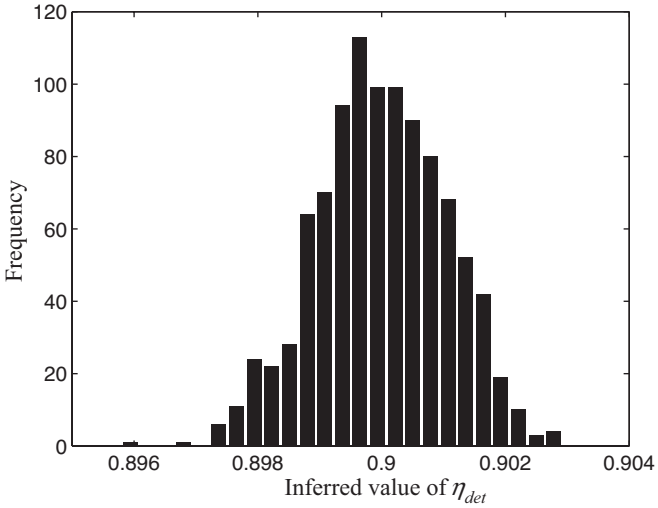

FIG. 3. Histogram of the inferred values of the ion detection system efficiency η_{det} for 1000 runs of the calibration simulation with $\eta_{det} = 0.9$, electron detection system efficiency $\eta_{det,e} = 0.9$, ionization rate $\dot{N}_I = 10^4\ \mathrm{s}^{-1}$, calibration time $\tau_{cal} = 10$ s, pulse resolution time $\tau_r = 10$ ns, and background electron and ion detection rates $\dot{N}_{ib} = \dot{N}_{eb} = 10^2\ \mathrm{s}^{-1}$, respectively.

V. TRAP LOSS AND OPTIMAL IONIZATION RATE

In an atom-counting experiment it is important to know how the rate of ionization affects the normalized count uncertainty κ. The greater the rate of ionization, the smaller the value of p_r and the larger its uncertainty. This in turn decreases η_i and increases σ_{η_i}, resulting in an increased value of κ. However in most experiments it would generally be desirable to ionize a cloud as quickly as possible without overly affecting the count accuracy. Figure 4 shows how κ is affected by the ionization time $\tau_I \equiv N_I/\dot{N}_I$, for $N_I = 10^3$ and $\tau_r = 5$ ns, assumed to be known with a 10% uncertainty. The crosses correspond to an infinitely long ionization (in which case $\eta_i = \eta_{det}$) and the circles and triangles correspond to ionization times of 2 and 1 ms, respectively. It can be seen that down to a certain ionization time, κ is close to its minimum value. However as the ionization time decreases, κ begins to increase rapidly.

If there is negligible trap loss, the number of atoms ionized N_I is the same as the number of atoms originally in the trap N, and the inferred atom number N_{inf} is the same as the inferred ion number $N_{I,inf}$. If there is trap loss, however, we have to correct the inferred ion number to obtain an inferred atom number. In the remainder of this section we show how this is achieved and how the uncertainty in the inferred atom number is affected by trap loss. We also find the optimal ionization rate that minimizes the uncertainty in the inferred atom number due to both trap loss and imperfect ion temporal resolution.

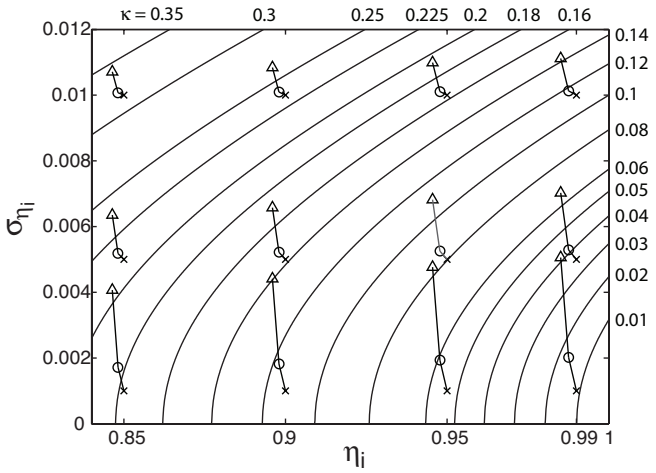

FIG. 4. Contour plot of the normalized count uncertainty κ, showing how κ increases as the ionization time τ_I decreases, for various combinations of initial values of the overall ion detection efficiency η_i and its uncertainty σ_{η_i}. Crosses, circles, and triangles correspond to $\tau_I \to \infty$, τ_I=2 ms and τ_I=1 ms, respectively.

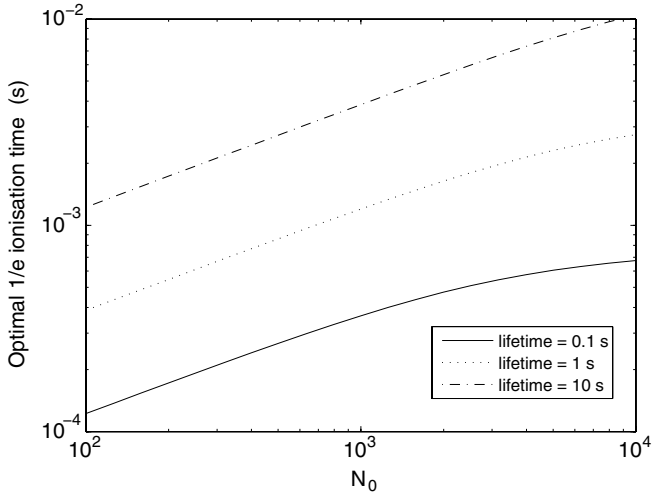

FIG. 5. The optimal $1/e$ time required to ionize the cloud is shown as a function of the atom number and the loss rate from the trap.

To calculate the atom count corrected for trap loss, we assume a constant loss rate R_l and that ionization occurs at a constant rate R_I (both rates are per atom). The respective time-dependent probabilities of an atom being in the trap and of having been ionized follow

$$\dot{P}_T = -(R_I + R_l)P_T, \tag{14}$$

$$\dot{P}_I = R_I P_T. \tag{15}$$

The probability that an atom is ionized rather than lost is

$$p_I = \int_0^\infty \dot{P}_I dt = \frac{R_I}{R_I + R_l}. \tag{16}$$

The total number of atoms ionized N_I is described by a binomial distribution, which again can be approximated by a normal distribution with mean $p_I N$ and standard deviation $\sqrt{p_I(1-p_I)N}$ [50]. The original number of atoms in the trap can then be inferred to be

$$N_{inf} = \left(1 + \frac{R_l}{R_I}\right) N_{I,inf}, \tag{17}$$

with a statistical uncertainty of

$$\sigma_{N_{inf},stat} = \sqrt{\frac{R_l}{R_I}\left(1 + \frac{R_l}{R_I}\right) N_{I,inf}}. \tag{18}$$

Due to uncertainties in R_l, R_I, and $N_{I,inf}$, we get extra terms in the uncertainty in N_{inf} and we find

$$\sigma_{N_{inf}}^2 = \left(\frac{N_{I,inf}\sigma_{R_l}}{R_I}\right)^2 + \left(\frac{R_l N_{I,inf}\sigma_{R_I}}{R_I^2}\right)^2 + \left[\left(1 + \frac{R_l}{R_I}\right)\sigma_{N_{I,inf}}\right]^2 + \frac{R_l}{R_I}\left(1 + \frac{R_l}{R_I}\right) N_{I,inf}, \tag{19}$$

with $N_{I,inf}$ and $\sigma_{N_{I,inf}}$ given by Eqs. (2) and (3). Thus in order to infer the atom number and its uncertainty, we need to know R_I and R_l and their uncertainties in addition to N_i, η_i, and σ_{η_i}. We now consider how these values can be measured in a given experiment.

The sum of R_I and R_l can be found by plotting $\ln[N_i - N_i(t)]$ against time, where $N_i(t)$ is the cumulative ion count. The slope is then $-(R_I + R_l)$. The value of R_l (and hence of R_I) may be found by plotting $R_I + R_l$ against the intensity of the 778 nm laser for a number of runs. R_l is given by the extrapolated y intercept of this plot. (Extrapolation is required because R_l cannot be measured by counting ions if no ionization occurs. However, R_l could be measured directly by absorption imaging at successive times in the absence of 778 nm light.)

The optimal ionization rate is that which gives the lowest value of κ for given values of R_l, η_{det}, τ_r, and N. In Fig. 5, the optimal value of $1/R_I$ is plotted as a function of N for various values of $1/R_l$, for η_{det}=0.9, σ_{η_i}=0, τ_r=10 ns, and assuming a 10% uncertainty in the measured values of R_l and R_I. The corresponding minimum values of κ/κ_{min} are plotted in Fig. 6, where κ_{min} is the value of κ for zero trap loss. It can be seen that reasonably sized atom clouds (10^3–10^4 atoms) can be counted in times on the order of 10 ms with close to the theoretical minimum count uncertainties for realistic trap lifetimes.

An improvement on the uncertainties resulting from ionizing with constant per atom probability would be obtained by increasing the 778 nm laser power during the ionization in such a way as to obtain a constant ionization rate in atoms/s. This would mean that the cloud would be ionized faster with less trap loss. The time dependent rate equations describing this scheme could be integrated numerically to determine the probability that an atom is ionized rather than lost, from which the original atom number and its uncertainty could be inferred.

VI. DISCUSSION

We now consider the application of our atom-counting scheme to the characterization of unknown atomic samples.

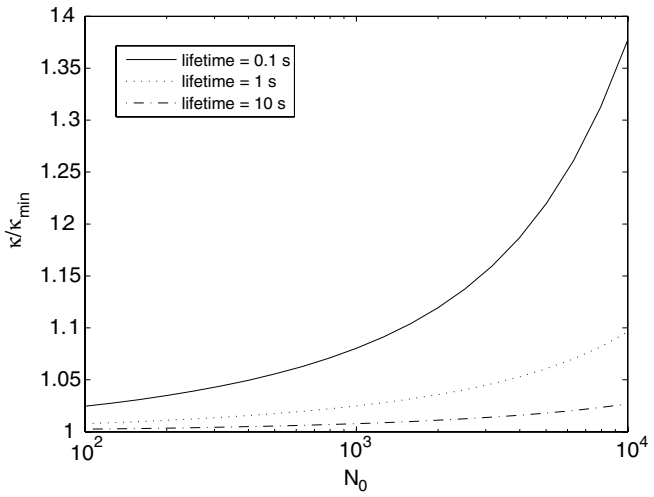

FIG. 6. The minimum achievable value of the relative count uncertainty κ expressed relative to κ_{min} (the value for zero loss) is shown as a function of atom number and trap lifetime. For the given values of the overall ion detection efficiency η_i and its uncertainty σ_{η_i}, $\kappa_{min} \approx 0.11$.

To determine the number of atoms in a single cloud, one would simply count a certain number of ions N_i and use the known calibration data to obtain an inferred atom number and uncertainty $N_{inf} \pm \sigma_{N_{inf}}$ from Eqs. (2) and (3). In the case that trap losses are not negligible, Eqs. (17) and (19) are also required. If, however, we wish to know the atom number variance in a specific situation we need to analyze a number of repeated measurements. As an example, consider a sample of n measurements on atom clouds generated in an identical manner which, under ideal (noise-free) circumstances, would yield identical numbers of atoms (for example, using a quantum tweezer to extract atoms from a BEC [32,33]). Each experiment yields a measure $N_{inf,j} \pm \sigma_{N_{inf,j}}$ where $j = 1, 2, \ldots, n$. The quantities of interest are the mean atom number, the atom number variance, and the uncertainties in these values.

The population mean can be estimated from the mean of all inferred atom numbers $\bar{N}$ and has an uncertainty of $\sqrt{s_T^2/n + (\sigma_{\eta_i}\bar{N}/\eta_i)^2}$ where s_T^2 is the bias-corrected sample total variance and is given by $s_T^2 = [1/(n-1)]\Sigma(N_{inf,j} - \bar{N})^2$. The true atom number variance σ_A^2 is estimated by the difference of the total variance of the measurements s_T^2 and the variance associated with the binomial statistics of the ion counting $\sigma_m^2 \cong \bar{N}(1-\eta_i)/\eta_i$. Note that the expression for σ_m^2 does not include a term due to σ_{η_i} as in Eq. (3), since we assume that any error in the detection efficiency (calibration) will be the same for each measurement. This leads to a systematic error in the atom count and does not contribute to the variance σ_m^2.

The degree of number squeezing of the atomic population is described by the Fano factor $F_A = \sigma_A^2/\bar{N}$ [54]. A Poissonian sample has $F_A = 1$ and a sub-Poissonian (number-squeezed) sample has $F_A < 1$. We can define a total Fano factor $F_T = s_T^2/\bar{N}$ and measurement Fano factor $F_m = \sigma_m^2/\bar{N}$, which accounts for the fluctuations due to the binomial counting of ions. The population Fano factor is then given by $F_A = F_T - F_m$, and it can be shown that for $\sigma_{\eta_i} < 5\%$ and $\bar{N} > 5$ the uncertainty in F_A is well approximated by $\sigma_{F_A} = \sqrt{2/n}(F_A + F_m)$.

Knowing F_m from the calibration it is possible to determine how many measurements are required to obtain a suitably small uncertainty σ_{F_A} in the measured (normalized) atomic variance F_A, or conversely, for a given number of measurements, to what accuracy F_A can be determined. For example, suppose 50 measurements are performed on an population that has $F_A = 0.2$, using a well-calibrated, 90% efficiency detector. The uncertainty in the inferred value of F_A is then 0.06. For mean atom numbers of 10^3 and 10^4, $F_A = 0.2$ corresponds to atom number standard deviations of 14 and 44, respectively. Given that $\sigma_{F_A} = 0.06$, these standard deviations can be measured to uncertainties of 3.1 and 9.8 atoms, respectively. Naturally, these uncertainties can be reduced by increasing the number of measurements. However since $\sigma_{F_A} \propto 1/\sqrt{n}$, a large number of measurements is required to substantially reduce these uncertainties. For example, if n is increased from 50 to 100, the uncertainties in the population standard deviations are only reduced to 2.2 and 7.0, respectively.

VII. CONCLUSION

We have analyzed photoionization and ion detection as a means of achieving accurate counting of ultracold atoms. The scheme relies on a three-photon, cw ionization process and can also be used for efficient single-atom detection with high spatiotemporal resolution. To count large numbers of atoms, one of the lasers acts as an optical dipole trap for the target atoms. We have shown that a well-calibrated ion detector with realistic efficiencies can achieve single-shot atom counts with sub-Poissonian accuracies for atomic samples containing many thousands of atoms. This is potentially useful for studies of the quantum properties of cold atomic gases. The variance of an ensemble of systems can also be characterized in a manner that only weakly depends on uncertainties in the absolute detection efficiency. Similarly, this scheme could allow direct probing of atom number correlations in molecular down-conversion and four-wave mixing experiments which are predicted to show number difference squeezing.

ACKNOWLEDGMENTS

This work was supported by the Australian Research Council, Landesstiftung Baden-Württemberg, and the European Union Grant No. MRTN-CT-2003-505032.

APPENDIX A: NET NUMBER OF FALSE COINCIDENCES

In this appendix we derive the required correction to a coincidence count to account for false coincidences and uncounted true coincidences. In a given calibration there will be $N_i - N_c$ unpartnered ions and $N_e - N_c$ unpartnered electrons. (We assume negligible background ion and electron numbers.) The probability of a given unpartnered ion being

in the window of an unpartnered electron is well approximated by

$$p_f = (N_e - N_c)\frac{\tau_{win}}{\tau_{cal}}, \tag{A1}$$

where τ_{win} is the window length and τ_{cal} is the duration of the calibration.

The probability of a true coincidence being outside the window is

$$p_w = 1 - \mathrm{erf}\left(\frac{\tau_{win}}{2\sqrt{2}\sigma_{int}}\right), \tag{A2}$$

where σ_{int} is the the standard deviation of the time intervals between electrons and their corresponding ions.

The net number of false coincidences counted in a given calibration is then

$$N_f = \bar{N}_f \pm \sigma_f, \tag{A3}$$

where

$$\bar{N}_f = p_f(N_i - N_c) - p_w N_c \tag{A4}$$

and

$$\sigma_f = \sqrt{p_f(1-p_f)(N_i - N_c) + p_w(1-p_w)N_c}. \tag{A5}$$

APPENDIX B: CALCULATION OF p_r AND p_r'

As the overall ion detection efficiency η_i is ionization rate dependent, relating the ion detection efficiency measured in a calibration to the ion detection efficiency which applies in an experiment requires finding an expression for p_r in terms of the ionization rate [see Eq. (1)]. We consider two cases: constant ionization rate in atoms per second, and constant per atom ionization rate. We look first at the former.

We assume the ion detection system has some resolution time τ_r, such that if an ion arrives at the detector within τ_r of the previous ion it will not be counted. We define $\dot{N}_i^*$ as the average rate (ions/s) at which ions are detected as $\tau_r \to 0$. Assuming a constant average detection rate, the detections follow Poissonian statistics, and the time interval between successive detections τ, is described by a negative exponential probability density function [50]

$$f_{int}(\tau) = \dot{N}_i^* e^{-\dot{N}_i^*\tau} \quad \text{for } \tau \geq 0. \tag{B1}$$

The probability that an ion arriving at the detector is resolvable from the previous ion is

$$p_r = 1 - \int_0^{\tau_r} f_{int}(\tau)d\tau. \tag{B2}$$

From Eqs. (B1) and (B2) we find

$$p_r = \exp(-\tau_r \dot{N}_i^*). \tag{B3}$$

The rate at which ions are actually detected is

$$\dot{N}_i = p_r \dot{N}_i^*. \tag{B4}$$

The number of ions counted during a calibration period τ_{cal} is described by a Poisson distribution: $N_i = \dot{N}_i\tau_{cal} \pm \sqrt{\dot{N}_i\tau_{cal}}$. If N_i ions are counted in time τ_{cal}, the ion detection rate in the calibration is inferred to be

$$\dot{N}_{i,cal} = \frac{N_i}{\tau_{cal}} \pm \frac{\sqrt{N_i}}{\tau_{cal}}. \tag{B5}$$

From Eqs. (B3) and (B4) we find

$$\dot{N}_i^* = (1 + \tau_r \dot{N}_i)\dot{N}_i + O((\tau_r \dot{N}_i)^3). \tag{B6}$$

Substituting Eq. (B6) into Eq. (B3) and neglecting the third-order term (which results in a relative error in p_r of less than 10^{-9} for $\tau_r \dot{N}_i < 10^{-3}$) we get

$$p_r = 1 - \tau_r \dot{N}_i - \frac{1}{2}(\tau_r \dot{N}_i)^2. \tag{B7}$$

Now we consider the case of ionization with a constant per atom ionization rate. In this case we need to use an effective ion resolution probability p_r' because by ionizing with a constant per atom rate, the ionization rate in ions per second is a function of time and hence so is p_r. The effective ion resolution probability is given by

$$p_r' = \int_0^\infty p_r(t) f_a(t) dt, \tag{B8}$$

where from Eqs (B3), (14), and (15)

$$p_r(t) = \exp(-\beta e^{-(R_I + R_l)t}), \tag{B9}$$

where $\beta = \tau_r \eta_{det} N R_I$ and

$$f_a(t) = (R_I + R_l)e^{-(R_I + R_l)t} \tag{B10}$$

is the probability density function of arrival times of ions at the detector. It can be shown that, neglecting terms of $O(\beta^3)$,

$$p_r' = 1 - \frac{1}{2}\beta + \frac{1}{3}\beta^2. \tag{B11}$$

[1] C. S. Adams, M. Siegel, and J. Mlynek, Phys. Rep. **240**, 143 (1994).

[2] M. Anderson, J. R. Ensher, M. R. Matthews, C. E. Wieman, and E. A. Cornell, Science **269**, 198 (1995).

[3] C. C. Bradley, C. A. Sackett, J. J. Tollett, and R. G. Hulet, Phys. Rev. Lett. **75**, 1687 (1995).

[4] K. B. Davis, M.-O. Mewes, M. R. Andrews, N. J. van Druten, D. S. Durfee, D. M. Kurn, and W. Ketterle, Phys. Rev. Lett. **75**, 3969 (1995).

[5] M. R. Andrews, C. G. Townsend, H. J. Miesner, D. S. Durfee, D. M. Kurn, and W. Ketterle, Science **275**, 637 (1997).

[6] M.-O. Mewes, M. R. Andrews, D. M. Kurn, D. S. Durfee, C.

G. Townsend, and W. Ketterle, Phys. Rev. Lett. **78**, 582 (1997).
[7] I. Bloch, T. W. Hänsch, and T. Esslinger, Phys. Rev. Lett. **82**, 3008 (1999).
[8] E. W. Hagley, L. Deng, M. Kozuma, M. Trippenbach, Y. B. Band, M. Edwards, M. Doery, P. S. Julienne, K. Helmerson, S. L. Rolston, and W. D. Phillips, Phys. Rev. Lett. **83**, 3112 (1999).
[9] Y. Le Coq, J. H. Thywissen, S. A. Rangwala, F. Gerbier, S. Richard, G. Delannoy, P. Bouyer, and A. Aspect, Phys. Rev. Lett. **87**, 170403 (2001).
[10] K. Mølmer, New J. Phys. **5**, 55 (2003).
[11] E. A. Burt, R. W. Ghrist, C. J. Myatt, M. J. Holland, E. A. Cornell, and C. E. Wieman, Phys. Rev. Lett. **79**, 337 (1997).
[12] B. L. Tolra, K. M. O'Hara, J. H. Huckans, W. D. Phillips, S. L. Rolston, and J. V. Porto, Phys. Rev. Lett. **92**, 190401 (2004).
[13] T. Kinoshita, T. Wenger, and D. S. Weiss, Phys. Rev. Lett. **95**, 190406 (2005).
[14] J. Esteve, J.-B. Trebbia, T. Schumm, A. Aspect, C. I. Westbrook, and I. Bouchoule, Phys. Rev. Lett. **96**, 130403 (2006).
[15] M. Schellekens, R. Hoppeler, A. Perrin, J. Viana Gomes, D. Boiron, A. Aspect, and C. I. Westbrook, Science **310**, 648 (2005).
[16] A. Öttl, S. Ritter, M. Köhl, and T. Esslinger, Phys. Rev. Lett. **95**, 090404 (2005).
[17] J. Javanainen and M. Y. Ivanov, Phys. Rev. A **60**, 2351 (1999).
[18] C. Orzel, A. K. Tuchman, M. L. Fenselau, M. Yasuda, and M. A. Kasevich, Science **291**, 238 (2001).
[19] M. Greiner, O. Mandel, T. Esslinger, T. W. Hänsch, and I. Bloch, Nature (London) **415**, 39 (2002).
[20] Z. Hadzibabic, S. Stock, B. Battelier, V. Bretin, and J. Dalibard, Phys. Rev. Lett. **93**, 180403 (2004).
[21] H. Pu and P. Meystre, Phys. Rev. Lett. **85**, 3987 (2000).
[22] L.-M. Duan, A. Sørensen, J. I. Cirac, and P. Zoller, Phys. Rev. Lett. **85**, 3991 (2000).
[23] A. Sørensen, L.-M Duan, J. I. Cirac, and P. Zoller, Nature (London) **409**, 63 (2001).
[24] D. C. Roberts, T. Gasenzer, and K. Burnett, J. Phys. B **35**, L113 (2002).
[25] K. V. Kheruntsyan and P. D. Drummond, Phys. Rev. A **66**, 031602(R) (2002).
[26] K. V. Kheruntsyan, Phys. Rev. A **71**, 053609 (2005).
[27] L. Deng, E. W. Hagley, J. Wen, M. Trippenbach, Y. Band, P. S. Julienne, J. E. Simsarian, K. Helmerson, S. L. Rolston, and W. D. Phillips, Nature (London) **398**, 218 (1999).
[28] G. K. Campbell, J. Mun, M. Boyd, E. W. Streed, W. Ketterle, and D. E Pritchard, Phys. Rev. Lett. **96**, 020406 (2006).
[29] S. Inouye, T. Pfau, S. Gupta, A. P. Chikkatur, A. Grlitz, D. E. Pritchard, and W. Ketterle, Nature (London) **402**, 641 (1999).
[30] M. Greiner, C. A. Regal, J. T. Stewart, and D. S. Jin, Phys. Rev. Lett. **94**, 110401 (2005).
[31] S. Fölling, F. Gerbier, A. Widera, O. Mandel, T. Gericke, and I. Bloch, Nature (London) **434**, 481 (2005).
[32] R. B. Diener, B. Wu, M. G. Raizen, and Q. Niu, Phys. Rev. Lett. **89**, 070401 (2002).
[33] C. S. Chuu, F. Schreck, T. P. Meyrath, J. L. Hanssen, G. N. Price, and M. G. Raizen, Phys. Rev. Lett. **95**, 260403 (2005).
[34] D. Frese, B. Ueberholz, S. Kuhr, W. Alt, D. Schrader, V. Gomer, and D. Meschede, Phys. Rev. Lett. **85**, 3777 (2000).
[35] N. Schlosser, G. Reymond, I. E. Protsenko, and P. Grangier, Nature (London) **411**, 1024 (2001).
[36] I. Teper, Y.-J. Lin, and V. Vuletić, e-print cond-mat/0603675.
[37] P. W. H. Pinkse, T. Fischer, P. Maunz, and G. Rempe, Nature (London) **404**, 365 (2000).
[38] C. J. Hood, T. W. Lynn, A. C. Doherty, A. S. Parkins, and H. J. Kimble, Science **287**, 1457 (2000).
[39] H. Mabuchi and A. C. Doherty, Science **298**, 1372 (2002).
[40] P. Horak, B. G. Klappauf, A. Haase, R. Folman, J. Schmiedmayer, P. Domokos, and E. A. Hinds, Phys. Rev. A **67**, 043806 (2003).
[41] J. E. Lye, J. J. Hope, and J. D. Close, Phys. Rev. A **67**, 043609 (2003).
[42] K. G. H. Baldwin, Contemp. Phys. **46**, 105 (2005).
[43] A. Ruschhaupt, B. Navarro, and J. G. Muga, J. Phys. B **37**, L313 (2004).
[44] T. Ristroph, A. Goodsell, J. A. Golovchenko, and L. V. Hau, Phys. Rev. Lett. **94**, 066102 (2005).
[45] J. Fricke, A. Müller, and E. Salzborn, Nucl. Instrum. Methods **175**, 379 (1980).
[46] I. P. Gilmore and M. P. Seah, Appl. Surf. Sci. **144-145**, 113 (1999).
[47] M. Frank, C. A. Mears, S. E. Labov, W. H. Benner, D. Horn, J. M. Jaklevic, and A. T. Barfknecht, Rapid Commun. Mass Spectrom. **10**, 1946 (1996).
[48] B. C. Duncan, V. Sanchez-Villicana, P. L. Gould, and H. R. Sadeghpour, Phys. Rev. A **63**, 043411 (2001).
[49] D. Ciampini, M. Anderlini, J. H. Müller, F. Fuso, O. Morsch, J. W. Thomsen, and E. Arimondo, Phys. Rev. A **66**, 043409 (2002).
[50] G. Knoll, *Radiation Detection and Measurement* (Wiley, New York, 1979).
[51] National Council on Radiation Protection & Measurements Report No. 58, 1985.
[52] Ortec 100-ps Time Digitizer/MCS Model 9395.
[53] S. Kraft, Ph.D. thesis, Universität Tübingen, 2006 (unpublished). Details will be published elsewhere.
[54] U. Fano, Phys. Rev. **72**, 26 (1947).